# **Recovery of Multicomponent Shale Gas from Single Nanopores**

Haiyi Wu, Yadong He, and Rui Qiao\* Department of Mechanical Engineering, Virginia Tech, Blacksburg, VA 24061

#### **ABSTRACT**

The adsorption of multicomponent gas mixtures in shale formations and their recovery are of great interest to the shale gas industry. Here we report molecular dynamics simulations of the adsorption of methane/ethane mixtures in 2nm- and 4nm-wide nanopores and their recovery from these nanopores. Surface adsorption contributes significantly to the storage of methane and ethane inside the pores, and ethane is enriched inside the nanopores in equilibrium with bulk methane-ethane mixtures. The enrichment of ethane is enhanced as the pore is narrowed, but is weakened as the pressure increases due to entropic effects. These effects are captured by the ideal adsorbed solution (IAS) theory, but the theory overestimates the adsorption of both gases. Upon opening the mouth of the nanopores to gas baths with lower pressure, both gases enter the bath. The production rates of both gases shows only weak deviation from the square root scaling law before the gas diffusion front reaches the dead end of the pores. The ratio of the production rate of ethane and methane is close to their initial mole ratio inside the nanopore despite that diffusion of ethane is slower than that of methane inside the pores. Scale analysis and calculation of the Onsager coefficients for the transport of binary mixture of methane and ethane inside the nanopores suggest that the strong coupling between methane and ethane transport is responsible for the apparently effective recovery of ethane from the nanopores.

<sup>\*</sup> Corresponding author. Email: ruigiao@vt.edu.

### I. INTRODUCTION

Natural gas production from shale formations has received extensive attention recently and can potentially lead to a new global energy source. The U.S. Energy Information Administration shows that shale gas provides the largest source of the growth in U.S. natural gas supply during the past decade, and its share is expected to grow continuously in the future. The composition of shale gas varies with among shale reservoirs. While methane is always the most abundant component in shale gas, hydrocarbons with higher molecular weight are also present. In particular, ethane is the usually the second primary component in shale gas and can account for up to 15 vol% of the recovered gas. The effective extraction of these hydrocarbons, which are much more valuable than methane, is of great interest for the shale gas industry.

A distinguishing feature of shale formations is that, while it typically features pores ranging from sub-nanometer to millimeters in size, its porosity is often dominated by nanopores smaller than 10-100 nanometers. As such, much of the gas is stored inside narrow nanopores as adsorbed gas and free gas.<sup>3, 4</sup> Based on extensive research on transport of fluids in nanopores<sup>5, 6</sup>, e.g., layering of fluids on pore walls modulates their transport through narrow pores<sup>7-10</sup>, one can expect that the thermodynamic and hydrodynamic properties of gas inside such pores, which govern the extraction of gases from the pores, can be quite different from those of bulk gas.<sup>11</sup> Tremendous progress has been made for understanding the adsorption and transport of single-component gas (usually methane) inside nanopores<sup>12, 13</sup> in the past decade, but those of multicomponent gas mixtures are much less well understood. Among the available studies,<sup>14-19</sup> much attention is focused on the competitive adsorption of CH<sub>4</sub>/N<sub>2</sub>/CO<sub>2</sub> gas species in shales, which plays an important role for enhancing shale gas recovery. However, a general understanding of the adsorption and transport of multicomponent shale gas under realistic reservoir condition (e.g., considering CH<sub>4</sub>/C<sub>2</sub>H<sub>6</sub> mixture) is still limited.

Research on the adsorption and transport of multicomponent shale gas in nanopores can potentially benefit from the extensive work on the thermodynamic and transport properties of multicomponent gas in other industrial applications.<sup>12, 19-25</sup> For example, previous studies have attempted to predicted the multicomponent adsorption via the Extend Langmuir (EL) model<sup>23</sup> and the Ideal Adsorbed Solution (IAS) model.<sup>22, 24</sup> In addition to these theoretical models, previous simulations also indicated that there exits complex competition between the adsorbed species. <sup>19-21</sup>

We are interested in understanding the storage of multicomponent gas mixtures in shale formations and their recovery during gas extraction using numerical simulation. Simulation of shale gas storage and recovery in shale formations appears extremely difficult because of the vast spectrum of pore sizes involved, the diverse surface chemistry of the pores, and the complicated connectivity between nanopores. Nevertheless, prior studies<sup>26, 27</sup> show that the overall shale gas recovery is mainly controlled by the transport of gas from the narrow pores to wide secondary fractures, and the essential features of shale gas adsorption and transport inside nanopores can be well captured by pore scale modeling with simple pore geometries, e.g. cylindrical or slit pores.<sup>26</sup> In this work, we study the adsorption of CH<sub>4</sub>/C<sub>2</sub>H<sub>6</sub> gas mixtures in single nanopores and their subsequent recovery from these pores using molecular dynamic (MD) simulation. In particular, we focus on the competitive adsorption effect of the two gases in the adsorbed phase of the nanopore and the gas recovery behavior of each species from the nanopore. Our work is inspired in part by prior studies on recovery of multicomponent shale gas, 16, 20, 21, 28 which have provided many useful insights into the dynamic behavior of gas adsorption and transport with mixtures components. Nevertheless, some important issues have not been addressed yet in these studies. For example, the competitive adsorption of CH<sub>4</sub>/C<sub>2</sub>H<sub>6</sub> gas inside nanopores and its impacts on shale gas storage is still not well understood, and a molecular view of the recovery of multicomponent gas mixture from nanopores is not yet available. By using MD simulations to study the gas recovery from nanopores, we will explicitly address these issues.

The rest of the paper is organized as follows: In Sec. II, we introduce the model and methods for simulations of the equilibrium isotherm and dynamic extraction of  $CH_4/C_2H_6$  mixture from

single nanopores. In Sec III, we present our simulation results on adsorption isotherm (with a focus on the competition between methane and ethane in the adsorbed phase) and the recovery characteristics of the two gases (with a focus on the recovery of ethane). Finally, conclusions are drawn in Sec. IV.

#### II. MD SIMULATION DETAILS

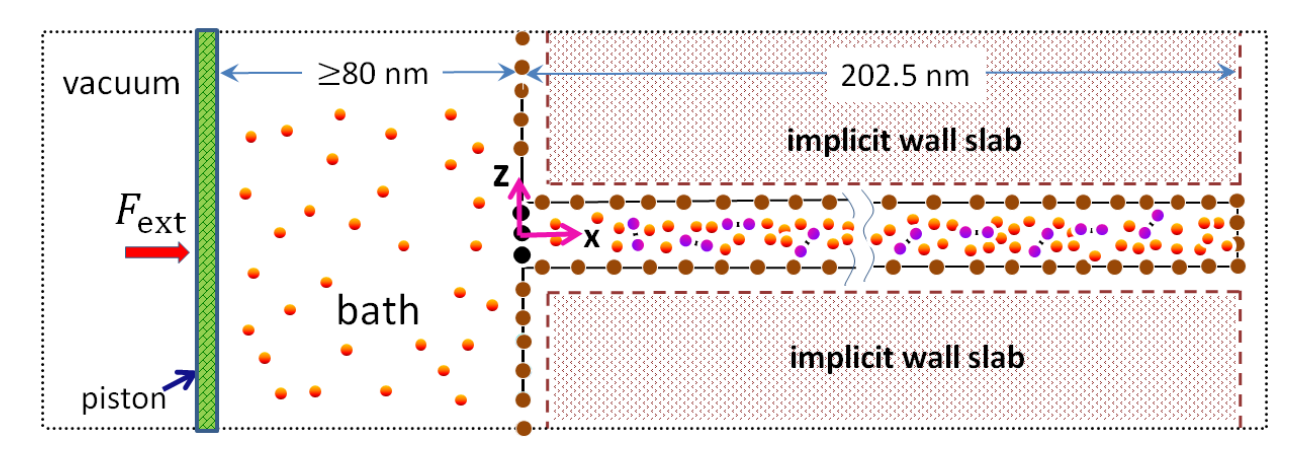


**Fig. 1.** A schematic of the MD system used for studying the adsorption of  $CH_4 - C_2H_6$  gas mixture in a single nanopore and their recovery from the pore. The simulation box is denoted using the black dotted lines. The brown spheres denote the explicitly modeled wall atoms and the shaded regions denote the implicit pore walls (see text for details). The black spheres at the pore mouth are the "blocker" atoms. The orange spheres and the purple dumbbells are the  $CH_4$  and  $C_2H_6$  molecules, respectively. The green plate at the left end side denotes the piston used to control the pressure in the gas bath.

Figure 1 shows a schematic of the MD system. The system features a slit pore, a gas bath with a constant pressure, a piston, and the shale gas molecules inside the pore and the gas bath. The system is periodical in the y- and z- directions. The pore's right end is permanently sealed. The center-to-center widths d of the investigated nanopores are 2nm and 4nm since pores with such small size are abundant in shale formations.<sup>26, 29</sup> Due to the finite size of the methane molecules and the wall atoms, the accessible pore width in MD model  $W_p$  is about 1.62 nm and 3.62 nm, respectively. The pore length L is 202.5 nm. The left side of the gas bath is bounded by a piston plate (green plate in Fig. 1), whose atoms move only in the x-direction. The constant gas pressure inside the gas bath is maintained by applying an external force  $F_{ext} = L_y L_z P_{bath}$  on

the piston plate ( $L_y = 13.5$  nm and  $L_z = 12.8$  nm are the plate's width in y- and z-directions, respectively;  $P_{bath}$  is the desired gas pressure inside the bath). All forces experienced by the piston plate are averaged and re-distributed evenly on the atoms of the piston plate such that the plate remains planar.

Two types of simulations are performed: adsorption isotherm simulations and gas recovery simulations. For the adsorption isotherm simulations, initially methane and ethane molecules are placed in the gas bath and equilibrated; the pore is empty and sealed by "blocker" atoms at its mouth (see the black spheres in Fig. 1). During the simulations, the pore is made open by removing the "blocker" atoms at its mouth, thus gas molecules move from the gas bath into the nanopore till a new equilibrium is reached. By using a gas bath that is sufficiently large and adjusting the number of gas molecules inside the gas bath by trial and error, the mole fraction of methane and ethane molecules inside the gas bath have been controlled to be 4:1 within a few percent. The amount of methane and ethane adsorbed inside the nanopore from the equilibrium run is used to determine the gas reserve inside the nanopore

For the gas recovery simulations, the system is setup with pure methane in the gas bath and gas mixtures ( $CH_4$ :  $C_2H_6$  molar ratio is 4:1) in the pore. Initially, the left end of the pore is sealed, and the system is equilibrated with higher pressure ( $P_0 = 200$  bar) in the pore and lower pressure in the bath ( $P_{bath} = 20$  bar). At t = 0, the "blocker" atoms at the left end of the pore are removed. Because the initial pressure inside the pore is higher than that in the gas bath, gas recovery is initiated.

Methane and ethane molecules are modeled using the TraPPE Force Field.<sup>30</sup> Briefly, methane molecules are modeled as structureless, spherical molecules; ethane molecules are modeled as dumbbell-shaped molecules featuring two united atoms each representing one CH<sub>3</sub> site, and the two united atoms are separated by a bond length of 1.54Å. While it is desirable to explicitly resolve all hydrogen atoms in the methane and ethane molecules, prior works show that the united atom approach taken here already allows accurate prediction of gas adsorption on planar

walls well with lower computational cost.<sup>6,20</sup> The inter-molecular interactions between an atom "m" and another atom "j" are modeled using the Lennard-Jones (LJ) potential,

$$\phi_{mj} = 4\epsilon_{mj} \left[ \left( \frac{\sigma_{mj}}{r} \right)^{12} - \left( \frac{\sigma_{mj}}{r} \right)^{6} \right] \tag{1}$$

where  $\sigma_{mj}$  and  $\epsilon_{mj}$  are the LJ parameters for the pair (m,j), and r is the distance between the two atoms. The piston plate is modeled as a square lattice of carbon atoms (lattice spacing: 0.3 nm). We confirmed that the simulation results are independent of the piston mass. Following Ref. 31, the pore walls are modeled as semi-infinite slabs constructed from a FCC lattice oriented in the <111> direction and the lattice constant is 0.54 nm. To avoid the significant computational cost of explicitly simulating all wall atoms, only the innermost layer of the wall atoms (i.e., the layer in contact with gas molecules) is explicitly modeled. The wall atoms beneath this layer are treated collectively as an implicit slab, and gas molecules inside the system interact with the implicit slab of wall atoms (the shaded region in Fig. 1) via an effective interaction described by the LJ 9-3 potential,

$$\phi_{m-iw} = \frac{2}{3}\pi\rho_w \epsilon_{mw} \sigma_{mw}^3 \left[ \frac{2}{15} \left( \frac{\sigma_{mw}}{r_0} \right)^9 - \left( \frac{\sigma_{mw}}{r_0} \right)^3 \right]$$
 (2)

where  $\rho_{\rm w}$  is the number density of the wall atoms in the implicit slab,  $\epsilon_{mw}$  and  $\sigma_{mw}$  are the LJ parameters for the interactions between the wall atoms and the gas molecules, and  $r_0$  is the closest distance between a gas particle and the surface of the implicit slab. The LJ parameters for the gas molecules and the wall atoms are summarized in Table 1.30 The interaction parameters for the methane-ethane (i.e., CH<sub>4</sub>-CH<sub>3</sub>) pair are determined from those for the CH<sub>4</sub>-CH<sub>4</sub> and CH<sub>3</sub>-CH<sub>3</sub> pairs using the Lorentz-Berthelot combination rule. With the structure of the wall and the LJ parameters for gas-wall interactions chosen here, the adsorption behavior of pure methane is found to be similar to those found in prior studies of methane adsorption in organic shale pores.<sup>32</sup>

**Table 1.** Lennard-Jones parameters for interactions between atoms.

	Parameters		
atom pair	$\sigma$ (nm)	$\epsilon/k_B$ (K)	
methane-methane	0.3730	148.0	
ethane-ethane <sup>a</sup>	0.3750	98.0	
methane-wall	0.3315	207.2	
ethane-wall <sup>b</sup>	0.3325	168.6	

<sup>&</sup>lt;sup>a</sup> this is for the interactions between the CH<sub>3</sub> sites of two different ethane molecules.

Simulations are performed using the Lammps code<sup>33</sup> with a time step size of 2 fs. The cut-off lengths for gas-gas interactions and gas-wall interactions are 1.4 nm and 1.5 nm, respectively. For each simulation, the volume of the system and the number of gas molecules inside the entire system are both kept constant. The pore wall atoms are fixed. We emphasize that, although the dimensions of the simulation box are fixed, the volume of the gas bath can change during gas recovery and adsorption isotherm simulations because its pressure is maintained by the piston (the simulation box is large enough in the x-direction so that the piston plate never protrudes out of the left boundary of the simulation box). The temperature of the gas molecules is maintained at 353 K using the Nose-Hoover thermostat. In each simulation, the density, pressure, and temperature of gas in both the nanopore and the gas bath are computed on-the-fly. Each simulation is repeated three times with different initial configurations to obtain reliable statistics. Specifically, before gas recovery simulations start, the gas molecules in the bath and in the pore are separated by the blocker atoms (see Fig. 1) and the system is equilibrated for 2 ns. The configurations of the system at three time instants (1.0, 1.5, and 2.0 ns) of the equilibrium run are saved. We then perform three gas recovery simulations, in which the initial configuration is taken from those three equilibrium configurations just saved.

b this is for the interactions between wall atom and one CH3 site of an ethane molecule.

## III. RESULTS AND DISCUSSION

### A. Methane and ethane storage in nanopores

As customary in studying material adsorption in porous materials, the storage of a gas species i inside a nanopore is measured per unit surface area of the pore using

$$n_{i,tot} = \frac{1}{2} \int_{-W/2}^{W/2} \rho_i(z) dz$$
 (3)

where  $\rho_i(z)$  is the density of the species across the pore, W is the pore width, and the factor 1/2 appears because each slit pore has two walls. Because the gas density is strongly inhomogeneous across nanopores (see, for example, the methane density profile in the inset of Fig. 2b), researchers often partition shale gas inside nanopores into adsorbed gas and free gas.<sup>3,4</sup> To delineate these two forms of gas and to help understand the storage of methane-ethane mixture in nanopores, we first examine the storage of pure methane and pure ethane in nanopores. Here, gas molecules in the density peaks next to the wall (shaded region in the inset of Fig. 2b, hereafter referred to as the adsorption layer) are taken as adsorbed gas and said to belong to the adsorbed phase. The rest of the gas molecules inside the pore are considered as free gas and said to belong to the free phase. The adsorbed gas of species i is quantified using

$$n_{i,ads} = \int_{-W/2}^{-W/2+\delta} \rho_i(z) dz = \int_{W/2-\delta}^{W/2} \rho_i(z) dz$$
 (4)

 $\delta$  is the thickness of adsorbed gas layer in z-direction (taken as 4 Å here). In principle,  $\delta$  may vary with pore size and pressure. However, examination of the gas density profiles in different pores at various pressures (see Fig. S3 in the Supporting Information) showed that, within the parameter space explored here, such variation is small and can be safely neglected.

Figure 2a shows the isotherm of the methane storage inside a 2.0nm-wide pore and its contribution by free and adsorbed gases. We observe that the adsorbed methane accounts for more than 60% of all methane stored inside 2.0nm-wide pores in the range of pressure investigated here, and their contribution increases as the pressure decreases. Similar trends are

observed when pure ethane is stored inside the same pore (see Fig. S1). However, as shown in Fig. 2b, at the same pressure, the amount of ethane adsorbed on the walls of 2nm-wide pores is larger than that of methane. This is expected because the adsorption of gas molecules on pore walls is driven by the attractive van der Waals forces between the gas molecules and the wall, and ethane molecules, which contain two CH<sub>3</sub> sites, have stronger van der Waals interactions with wall than methane molecules. The stronger adsorption of ethane on pore walls is also observed in the 4nm-wide pores (see Fig. S2).

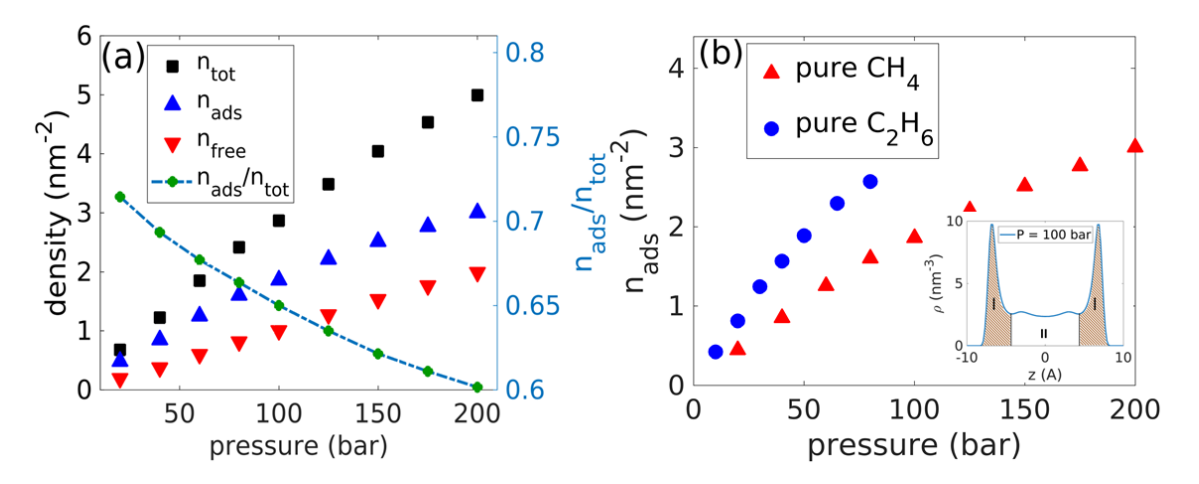


**Fig. 2**. (a) Isotherm of the storage of methane in 2nm-wide nanopores in equilibrium with a pure methane bath and the contribution by the adsorbed and free gas to the total gas storage. (b) Isotherms of methane and ethane adsorbed on the walls of a 2nm-wide nanopore when the pore is in equilibrium with pure methane and ethane gas bath. The inset is the density profile of methane across a 2nm-wide slit pore when the pore pressure is 100bar. Gas molecules in the region I (region II) are taken as the adsorbed (free) gas.

Next, we examine the gas storage inside nanopores in equilibrium with bath of binary methane-ethane mixtures. In all cases studied, the mole fraction of ethane in the gas bath is set to  $0.2\pm0.01$ . Figure 3a compares the storage of methane and ethane in a 2nm-wide pore as a function of pressure (data for methane-ethane mixture storage in 4nm-wide pore exhibits similar trend and is shown in Fig. S4). The nonlinear increase of the gas storage with pressure, a signature of significant contribution of surface adsorption to gas storage, is similar to that of pure gas. Figure 3b shows that the molecular fraction of ethane inside the nanopores is higher than that in the bath, i.e., ethane is enriched in the pores. The enrichment is stronger in the 2nm-wide

pores. Figure 3c further shows that, in both 2nm- and 4nm-wide pores, the enrichment of ethane inside pores is mainly caused by its enrichment in the wall-adsorbed phase. The latter is expected based on the results shown in Fig. 2b. However, Fig. 3c shows that the ethane enrichment decrease as the pressure increases beyond ~100 bar. This means that the adsorption of methane on the pore walls becomes more competitive than ethane as pressure increases beyond 100bar. To better understand this result, we examine the isotherm for the concurrent adsorption of methane and ethane on the walls of 2nm-wide pore.

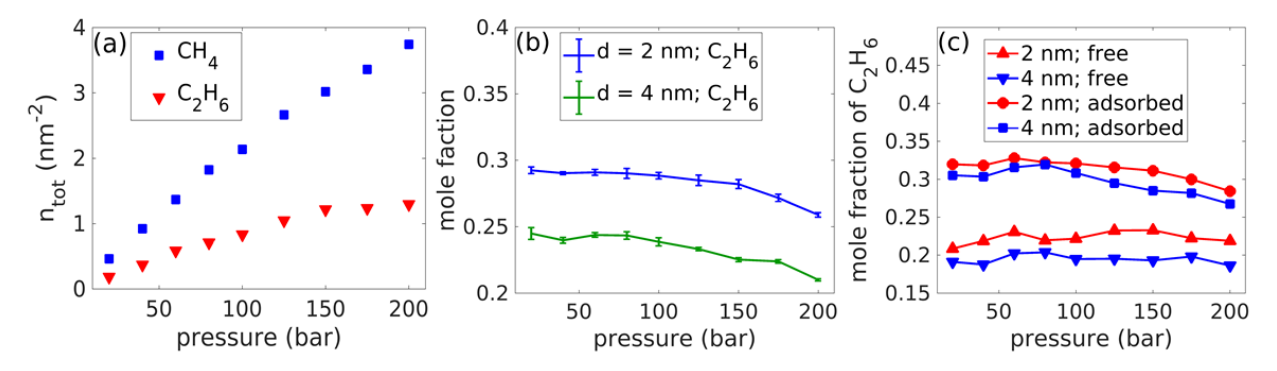
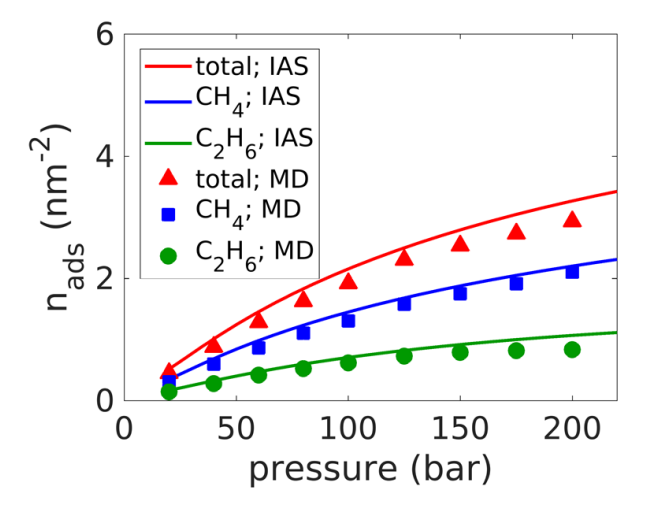


Fig. 3. (a) Isotherm of the methane and ethane storage inside a 2.0nm-wide pore. (b) Mole fraction of ethane inside pores with different widths. (c) Mole fraction of free and wall-adsorbed ethane inside pores with different widths. All pores are in equilibrium with a bath of binary methane-ethane mixture (mole fraction of ethane is  $0.2\pm0.01$ ).

Figure 4 shows the isotherms for the adsorption of methane and ethane on the walls of 2.0nm-wide pores. At P≲100bar, the adsorption of methane and ethane increases rapidly with pressure. As pressure increases further, the increase of the adsorption of both methane and ethane slows down. However, the slowdown is much more distinct for ethane and the adsorption of ethane reaches a plateau at P~150bar. In another word, ethane becomes less competitive in adsorbing on the pore walls than methane, and this leads to the reduced ethane enrichment at elevated pressure (see Fig. 3c). The less competitive adsorption of ethane than methane at high pressure can be understood as follows. At low to moderate pressure, the gas adsorption layer on the wall is loosely packed, and gas-wall interactions play the most important role in determining gas adsorption. Since ethane molecules interact more strongly with the pore walls than the

methane molecules, they outcompete methane in adsorption on pore walls. As the pressure increases, the gas adsorption layer becomes more densely packed and the entropic effects become more important. Since ethane molecules are larger than methane molecules, their entropy is lower than that of the methane molecules at elevated pressure. Therefore, ethane molecules become less competitive in adsorption on pore walls than the methane molecules. We note that a similar effect has been predicted theoretically in prior studies of binary adsorption of methane-ethane in zeolites.<sup>34-36</sup>



**Fig. 4.** Isotherm of methane and ethane adsorption on walls of a 2.0nm-wide pore predicted by MD simulations and the IAS theory. The pore is in equilibrium with a bath of binary methane-ethane mixture (mole fraction of ethane is  $0.2\pm0.01$ ). Results for methane/ethane adsorption on walls of 4.0nm-wide pore are similar and shown in Fig. S4.

We next investigate to what extent the isotherms computed using MD simulations can be predicted using existing theories. Among the available theories on multicomponent gas adsorption, the ideal adsorbed solution (IAS) theory<sup>24</sup> is popular due to its simplicity and good predicting power. The theory introduces a two dimensional confinement pressure termed spreading pressure in the adsorbed gas phase. By assuming that the different gas components are mixed ideally in the adsorbed gas phase and the area and enthalpy changes during mixing of different gas species are negligible for the same spreading pressure, the adsorption isotherm of different gas species (e.g., methane and ethane) on a solid substrate can be predicted using the

isotherms for the adsorption of pure gases (e.g., methane and ethane) as input. Using the adsorption isotherm of pure methane and ethane shown in Fig. 2, the adsorption of methane and ethane on the wall of a 2nm-wide pore in equilibrium with a binary mixture of methane and ethane (ethane mole fraction: 0.2) is determined using the IAS theory. Figure 4 shows that the IAS theory captures key feature of the isotherm of mixture adsorption on pore walls. Most importantly, the theory predicts that, as pressure increases beyond ~100bar, the increase of the adsorption of ethane slows down more significantly than that of methane, i.e., ethane becomes less competitive in surface adsorption than methane. Nevertheless, the theory systematically overestimates the adsorption of both methane and ethane, especially at high pressure. Similar discrepancy between the IAS predictions and experimentally measured isotherms has been found in some prior work, <sup>14</sup> and it is likely caused by the non-ideality of mixing methane and ethane in the adsorption layer on the pore walls.

#### B. Methane and ethane recovery from nanopores

In this section, we study the recovery of gas from a single nanopore (d = 2 or 4 nm) to a large gas bath. As detailed in Section 2, initially, each nanopore is filled with a methane/ethane mixture ( $CH_4$ :  $C_2H_6$  molar ratio: 4:1; total pressure: 200 bar) and the gas bath contains pure methane. The pressure in the gas bath is maintained at 20 bar throughout the simulation. At t = 0, the blocker atoms at the pore mouth are removed to initiate the gas recovery.

To gain generalized insight into the kinetics of gas recovery using our MD simulations, we nondimensionalize the time using a characteristic time  $t_c$ . Since gas recovery from nanopore is generally considered as a diffusive process, following previous works,  $^{26,37}$   $t_c$  is chosen as

$$t_c = \frac{4L^2}{D_m^0/\mathrm{Kn}^0} \tag{5}$$

where L is the nanopore length,  $D_m^0$  and  $\mathrm{Kn}^0$  are the reference molecular diffusion coefficient and Knudsen number inside the pore prior to gas recovery.  $D_m^0$  and  $\mathrm{Kn}^0$  depend on the molecular properties of the gas species and the pore size. For nanopores filled with multiple gas species, it is difficult to define  $D_m^0$  and  $\mathrm{Kn}^0$ , and thus  $t_c$ , uniquely. Here, we use the molecular

properties of methane (cross-sectional area:  $0.45 \text{ nm}^2$ ) to calculate the characteristic time  $t_c$  since methane dominates the gas storage inside the nanopores. With the temperature and initial pressure inside the nanopores, we obtain a  $D_m^0$  of  $5.53 \times 10^{-8} \text{m/s}^2$ . Furthermore, we compute a mean free path corresponding to the initial pressure inside the pore ( $\lambda_0$ ) and a mean free path corresponding to the pressure inside the gas bath ( $\lambda_f$ ).  $\lambda_0$  is more relevant to the gas transport in the pore interior and at early stage of gas recovery;  $\lambda_f$  is more relevant to gas transport near pore mouth. It is found that  $\lambda_0 = 0.26 \text{ nm}$  and  $\lambda_f = 1.9 \text{ nm}$ . Using the accessible width of the pore as the characteristic length scale, the corresponding Knudsen numbers are found to be  $\text{Kn}^0 = 0.16$  and  $\text{Kn}^f = 1.19$  for the 2nm-wide pore. Note that the accessible width of a pore with a width of 2.0nm (4.0nm) measured between the center planes of the atoms in its two walls is 1.6nm (3.6nm) because the methane molecule has a diameter of ~0.4nm.

We first examine the qualitative features of gas recovery process. Figure 5a shows the methane density profile across the 4nm-wide pore at different x-positions at  $t/t_c=0.01$ . We observe that, both near the pore wall and in the central portion of the pore, methane density decreases from their initial values (marked using a dashed line in Fig. 5a), which suggests that the adsorbed gas and the free gas are recovered from the pore concurrently. The drop of the gas densities from their initial values becomes less significant as we move from the pore mouth toward the pore interior, which is indicative of the diffusive nature of the gas recovery process. Figure 5b shows the evolution of the cross-section averaged density profiles of methane and ethane along the pore length. After the gas recovery starts, the methane and ethane densities near the pore mouth drops quickly because of the gas exchange between the gas bath (where the gas density is lower) and the gas at the pore mouth. As gas recovery proceeds, gas density in the pore interior drops and clear diffusion front moving toward the pore interior is observed. The diffusion front reaches the pore's sealed end at  $t/t_c \sim 0.01$ , and the density of both methane and ethane decreases along the entire pore length after that. We note that the gas density at the pore mouth gradually decreases as gas recovery proceeds, which suggests that the gas exchange between the gas bath and pore mouth has a finite resistance. Such a resistance also manifests as

concentration polarization in the gas bath. Indeed, as shown in Fig. 5c, the densities of methane and ethane are non-uniform inside the gas bath, and a diffusion boundary layer in which the gas density varies sharply is visible near the pore mouth. The strength of concentration polarization, as indicated by the drop of gas density across the diffusion boundary layer, is comparable for methane and ethane. Because concentration polarization reduces the driving force for the gas transport from the pore to the gas bath, it slows down gas recovery. The nominal driving force for recovery of methane is larger than that for ethane because the maximal difference of the density of methane inside the pore and the gas bath (~4 nm<sup>-3</sup> according to Fig. 5b and 5c) is larger than that for ethane (~1 nm<sup>-3</sup> according to Fig. 5b and 5c). Because the strength of concentration polarization is similar for methane and ethane, concentration polarization likely slows down the recovery of ethane more notably than that of methane.

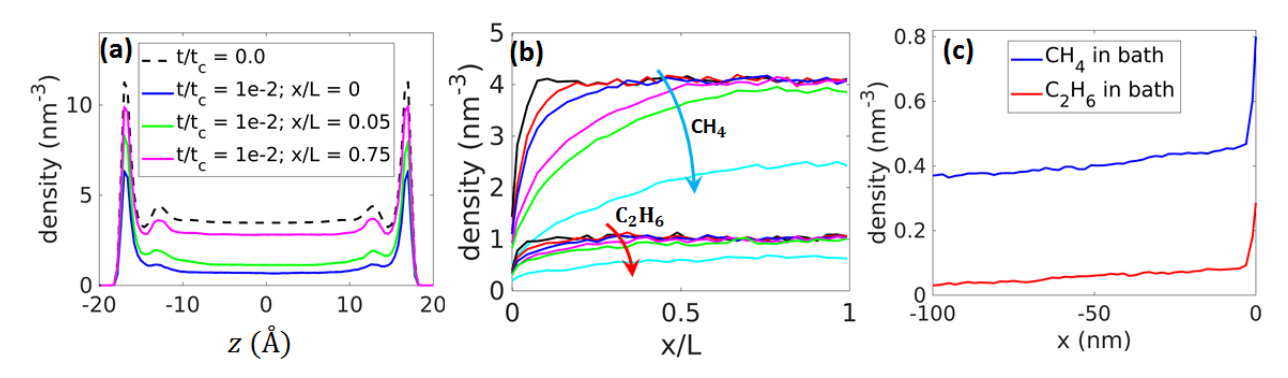


Fig. 5. Evolution of the density profiles of methane and ethane molecules inside the 4nm-wide pore and the gas bath during gas recovery. (a) Methane density profile across the nanopore at difference positions along the pore (x/L = 0, 0.05, 0.75) at  $t/t_c = 0.01$ . The dash line denotes the initial methane density across the pore. (b) The cross-section averaged density of methane and ethane along the pore length at  $t/t_c = 10^{-4}, 5 \times 10^{-4}, 10^{-3}, 5 \times 10^{-3}, 10^{-2}, 5 \times 10^{-2}$ . The arrows in the figure indicate the direction of increasing time. (c) Density of methane and ethane along the x-direction in the gas bath at time  $t/t_c = 0.01$  (x=0 corresponds to the position of the pore mouth, see Fig. 1).

Next, we investigated the production rate of methane and ethane during gas recovery process. The production rate of a gas species i is quantified as its flux out of a nanopore using

$$Q_i(\tilde{t}) = -dN_i/d\tilde{t} \tag{6}$$

where  $\tilde{t} = t/t_c$  is the dimensionless time and  $N_i$  is the number of species i's molecules inside

the pore. The fluxes of methane and ethane from the 2nm- and 4nm-wide pores are shown in Fig. 6a and 6b, respectively. At earlier time ( $\tilde{t} < 0.01$ ), the flux of both methane and ethane follow a superdiffusive scaling law  $Q(\tilde{t}) \sim \tilde{t}^{-\alpha}$  with  $0.4 < \alpha < 0.5$ , which differs from the  $Q(\tilde{t}) \sim \tilde{t}^{-0.5}$  for purely diffusive gas recovery. Similar deviation from the purely diffusive scaling law has been reported for the recovery of pure gas from nanopores, and is caused by the delayed removal of gas molecules adsorbed on the pore walls.<sup>37</sup> At  $\tilde{t} \gtrsim 0.04$  ( $\tilde{t} \gtrsim 0.01$ ), the production of methane and ethane from the 2nm-wide (4nm-wide) pore starts to deviate from the power law scaling behavior. This is consistent with the fact that the diffusion front reaches the pore's sealed end at these times (see Fig. 5b). Figure 6c shows the evolution of the ethane and methane flux ratio ( $Q_e/Q_m$ ) with time. We observe that, during the entire gas recovery operation,  $Q_e/Q_m$  is mostly in the range of 0.19-0.22, which is very close to the initial ethane-to-methane ratio of 0.25 inside the nanopores. This result is somewhat surprising. Specifically, because of the stronger attraction of ethane to the pore walls (and consequently stronger adsorption on the pore walls) than methane (see Fig. 3), the mobility of ethane molecules confined inside narrow pores is much smaller than that of the

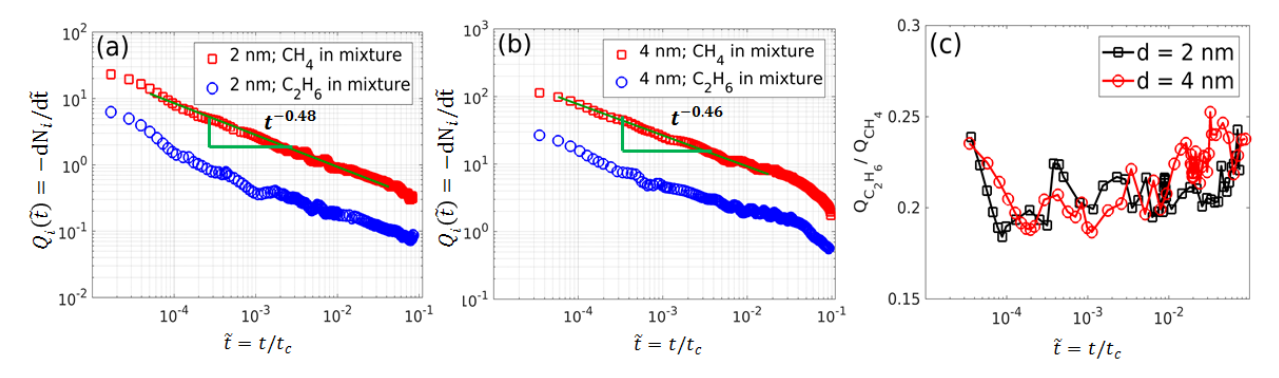


**Fig. 6.** (a-b) The evolution of the production rate of the methane and ethane compared with the pure methane from the 2nm-wide pore (a) and the 4nm-wide pore (b). (c) The evolution of the ratio of the methane and ethane flux out of the pore.

methane molecules. For example, we compute the total diffusion coefficient of methane (ethane) molecules confined inside 2nm- and 4nm-wide pores filled with pure methane (ethane) at various pressure (see Supporting Information), and find that the mean total diffusion coefficient of ethane molecules confined in these pores is 4-5 times smaller than that of the methane molecules at the

same pressure (see Fig. S5). In addition, as discussed earlier, the concentration polarization near the pore mouth likely slows down the recovery of the ethane more significantly than that of the methane. Therefore, one could have expected  $Q_e/Q_m$  to be much smaller than 0.25 during gas recovery. Below we seek to understand why this is not what we observed in the direct simulation of gas recovery from nanopores.

In principle, the composition of the gas recovered from pores filled with multiple gas species can be understood using several theoretical methods for describing multicomponent fluid transport, e.g., the Onsager formulism based on non-equilibrium thermodynamics and the Maxwell–Stefan formulism.<sup>38</sup> Here we adopt the Onsager formulism, in which the transport of two species i and j in a mixture can be described using

$$J_i = -L_{ii}\nabla\mu_i - L_{ij}\nabla\mu_i \tag{7}$$

where  $J_i$  and  $\mu_i$  are the flux and chemical potential of species i, respectively.  $L_{ij}$  is the Onsager coefficient, which depends on the concentration and distribution of species i and j in the mixture, as well as the interactions between gas species. Rigorous calculations of the gas fluxes from nanopores initially filled with multicomponent gas is complicated by the fact that, because the gas density and composition evolves both temporally and spatially inside the pore, the Onsager coefficients also vary temporally and spatially inside the pore and thus difficult to compute accurately. Here we combine scale analysis and MD simulations to obtain a semi-quantitative understanding of the composition of gas fluxes from pores during gas recovery operations.

Since the IAS theory predicts the isotherm of gas storage inside nanopores quite well (see Fig. 4), it is reasonable to assume that methane and ethane are mixed ideally inside the pore. We thus approximate the fugacity of gas species i using its partial pressure and write the chemical potential of species i as  $\mu_i - \mu_{i,0} = k_B T \ln(P_i/P_{i,0})$ , where  $\mu_{i,0}$  and  $P_{i,0}$  are the chemical potential and partial pressure of species i at a reference state, respectively.  $k_B T$  is the thermal energy. Further assuming that each gas inside the pore behaves ideally, the gradient of the

chemical potential of the species *i* can now be written as  $\nabla \mu_i = \rho_i^{-1} \nabla P_i$ , where  $\rho_i$  is the density of the species *i*. The flux of gas species *i* out of the nanopore,  $Q_i(t)$ , thus reads

$$Q_i(t) = A\left(-L_{ii}\rho_i^{-1}\nabla P_i - L_{ij}\rho_j^{-1}\nabla P_j\right)\Big|_m \tag{8}$$

where the subscript m indicates that the terms in the bracket should be evaluated at the pore mouth, and A is the cross-section area of the pore. Because the gas recovery rate drops sharply at late stage and is thus of limited interest for practical gas recovery operations, we focus on the early stage of the gas recovery operation when the diffusion front has not reached the pore's sealed end (i.e.,  $t/t_c < \sim 0.01$  in the pore considered here, see Fig. 5 and 6). In this case, the scale of  $\nabla P_i$  is given by

$$\nabla P_i \sim \left(P_{i,df} - P_{i,m}\right) / l_{df}(t) \tag{9}$$

where  $P_{i,df}$  and  $P_{i,m}$  are the partial pressure of species i at the diffusion front inside the pore and at the pore mouth, respectively (hereafter we denote methane and ethane as species "1" and "2", respectively).  $l_{df}(t)$  is the distance from the pore mouth to the diffusion front at time t. While  $\rho_i$  varies along the pore length during gas recovery, one can reasonably approximate it as the average of the gas density at the pore mouth and the diffusion front. Since gas is assumed to behave ideally, it follows that  $\rho_i \sim (k_B T)^{-1} (P_{i,df} + P_{i,m})/2$ .  $L_{ij}$  depends on the composition of gas species and their interactions inside the nanopores. As a first attempt, we approximate  $L_{ij}$  in Equ. 8 using the Onsager coefficients computed for methane and ethane mixture inside the 2nm-and 4nm-wide pores at the beginning of gas recovery when the pressure is 200 bar (see below), and denote  $L_{ij}$  thus obtained as  $L_{ij}^0$ . With the above assumptions and approximations, the flux of a gas species i at the pore mouth can be estimated as

$$Q_{i} \sim -\frac{2k_{B}T}{l_{df}(t)} \left( \frac{P_{i,df} - P_{i,m}}{P_{i,df} + P_{i,m}} L_{ii}^{0} + \frac{P_{j,df} - P_{j,m}}{P_{j,df} + P_{j,m}} L_{ij}^{0} \right)$$
(10)

The ratio of the ethane and methane flux from the nanopore can then be estimated as

$$Q_e/Q_m \sim \left(\frac{L_{21}^0}{L_{11}^0} + \frac{L_{22}^0}{L_{11}^0} G_{21}\right) / \left(1 + \frac{L_{12}^0}{L_{11}^0} G_{21}\right)$$
(11a)

$$G_{21} = (P_{2,df} - P_{2,m})(P_{1,df} + P_{1,m})/(P_{1,df} - P_{1,m})(P_{2,df} + P_{2,m})$$
(11b)

Taking advantage of the fact that gas bath contains mostly methane throughout the gas recovery operation and neglecting the concentration polarization at pore mouth, we have  $P_{1,m} \approx P_{bath} = 20$  bar and  $P_{2,m} \approx 0$ . Since the gas density at the diffusion front differs little from the gas densities inside the nanopore prior to gas recovery operations and we assume that methane and ethane are mixed ideally, we take  $P_{1,df} \approx P_0 x_1^0$  and  $P_{2,df} \approx P_0 x_2^0$ , where  $P_0$  is the pressure inside nanopore t = 0. Because the mole ratio of ethane and methane inside the nanopore is 1:4 at t = 0, we have  $x_1^0 = 0.8$  and  $x_2^0 = 0.2$ . It follows that  $G_{21} \approx 1.29$ .

To estimate  $Q_e/Q_m$  using Equ. 11, we next determine  $L_{11}^0$ ,  $L_{21}^0$ ,  $L_{12}^0$ , and  $L_{22}^0$  using the method introduced by previous researchers.<sup>28,39</sup> For a binary mixture of species i and j confined in a pore that is periodical in its length direction, one applies a constant force  $F_j$  on each molecule of species j in direction along the pore. By measuring the resulting fluxes of these species,  $L_{ij}$  can be computed using

$$L_{ij} = J_i/F_i = \bar{\rho}_i < v_i > /F_i \tag{12}$$

where  $J_i$ ,  $\bar{\rho}_i$ , and  $< v_i >$  are the flux, average density, and average velocity of species i in the pore. Here, we build nanopores with geometry and wall properties identical to those of the pores used in our gas recovery simulations except that these pores are periodical in their length direction. The pores are filled with ethane-methane mixture (mole ratio is 1:4) to a pressure of 200bar. To determine  $L_{11}^0$  and  $L_{21}^0$ , we apply a constant force  $F_1$  on each methane molecule inside the pore and compute the resulting fluxes of the methane and ethane molecules,  $L_{11}^0$ , and  $L_{21}^0$  using Equ. 12. Here we use  $F_1 = 0.143$ pN, and we also find that increasing or decreasing  $F_1$  by 3 times does not affect the computed  $L_{11}^0$  and  $L_{21}^0$  within statistical error.  $L_{22}^0$  and  $L_{12}^0$  are computed using similar methods.

Table 2 shows the computed Onsager coefficients. We observe that  $L^0_{12}$  is equal to  $L^0_{21}$ 

within statistical uncertainty, thus satisfying the Onsager reciprocity. The relative magnitude of the diagonal and off-diagonal terms depend only weakly on the pore size. The diagonal term  $L_{22}^0$  is much smaller than  $L_{11}^0$ , and this is consistent with the facts that there are much more methane molecules in the pore than ethane molecules and the total diffusion coefficient of methane molecules confined in nanopores is larger than that of the ethane molecules (see Fig. S5). Importantly, we observe that the cross-correlation  $L_{12}^0$  is even higher than the  $L_{22}^0$  term. This indicates that the interactions between methane and ethane play a critical role in the transport of ethane in the nanopores.

**Table 2.** The Onsager coefficients for the transport of methane (species 1) and ethane (species 2) inside slit nanopores with different widths.\*

	$L_{11}^0/L_{11}^0$	$L_{21}^0/L_{11}^0$	$L_{12}^0/L_{11}^0$	$L_{22}^0/L_{11}^0$
d = 2  nm	1	$0.19 \pm 0.01$	$0.18 \pm 0.01$	$0.08 \pm 0.01$
d = 4  nm	1	$0.21 \pm 0.01$	$0.20 \pm 0.01$	$0.06 \pm 0.01$

<sup>\*</sup> The nanopores are filled with methane and ethane with mole ratio of 1:4 and pressure of 200bar.

Using the Onsager coefficients shown in Table 2 and Equ. 11, the ratios of the ethane and methane fluxes  $(Q_e/Q_m)$  during gas recovery from 2nm- and 4nm-wide pores are estimated to be 0.219 and 0.220, respectively. These estimations are in good agreement with the results shown in Fig. 6c. The relatively large  $Q_e/Q_m$  originates from the facts that  $L_{21}^0$  is not much smaller than  $L_{11}^0$  and  $L_{12}^0$  is larger than  $L_{22}^0$ , both of which reflect the effective coupling between the transport of ethane and methane inside nanopores. In the above analysis, the effect of concentration polarization at the pore mouth is neglected. When such effect is taken into account by using the gas composition measured at pore mouth at representative time (e.g., at  $t/t_c = 0.01$ , see Fig. 5c) to determine  $P_{1,m}$  and  $P_{2,m}$  in Equ. 11b, the  $Q_e/Q_m$  predicted using Equ. 11a only decreases slightly (see Supporting Information).

## IV. CONCLUSIONS

We use MD simulations to investigate the adsorption of binary mixture of methane and ethane in nanopores and the gas recovery from these pores to low pressure gas bath. Calculation of the binary adsorption isotherm of nanopores in equilibrium with bulk methane-ethane mixture shows that while both methane and ethane are stored as free gas and adsorbed gas inside the nanopores, the adsorption of ethane on the wall is stronger than methane. The stronger adsorption of ethane on pore walls compared to methane leads to an enrichment of ethane inside nanopores. Such an enrichment is more pronounced in narrow pores but is weakened as the pressure increases due to entropic effects. During gas recovery operations, free and adsorbed gas are extracted concurrently from the nanopores, and noticeable concentration polarization, occurs near the pore mouth. Nevertheless, the production rates of both gases approximately follows the square root scaling law before the diffusion front reaches the sealed end of the nanopores. The ratio of the production rate of ethane and methane from the pores is only slightly smaller than their initial mole ratio inside the pores, which is attributed to the effective coupling of the transport of methane and ethane inside nanopores.

Our simulation results suggest that the storage of binary gas in narrow nanopores is affected strongly by the adsorption of different gas molecules on the wall, which depends on both the pore pressure and the nature of gas molecules. Since molecular simulations are computationally too costly for determining such adsorption in practical applications, molecular theories are needed. In this regard, we show that the classical IAS theory can predict the essential trends of binary gas adsorption on the pore walls, although it tends to overestimate the gas adsorption. Our simulations revealed that the recovery of binary gas mixture from single, narrow nanopores to gas baths is approximately a diffusive process and the coupling between the transport of gas species inside the nanopores plays an essential role in determining the composition of the recovered gas. These results lend support to the existing theories for gas recovery from nanopores and point to the need to develop effective models for predicting the coupling of the transport of different gas species confined inside nanopores.

Molecular simulations of gas recovery are limited to systems with pores many orders of magnitude shorter than in real shale formations, and this necessarily introduces some undesirable features such as extremely large pressure gradient along pore length and from the pore opening to the gas bath during gas recovery. Nevertheless, the fact that the present and our earlier MD simulations<sup>37</sup> capture the scaling law of gas recovery rate reported in field studies and continuum simulations<sup>26, 40</sup> suggests that these undesired features do not incur significant artifacts into the simulations. Therefore, MD simulations not only can be used to understand the transport and adsorption properties of gases in nanopores as demonstrated extensively in the past years, but can also be used as a powerful tool for exploring the essential physics of gas recovery process. In this study, we focus on the recovery of CH<sub>4</sub>-C<sub>2</sub>H<sub>6</sub> mixture from nanopores. The same method can be used for understanding the recovery of other gas mixtures. For example, since some shale formations contains a greater share of CO<sub>2</sub> than C<sub>2</sub>H<sub>6</sub>, it would be interesting to study the recovery of CH<sub>4</sub>-CO<sub>2</sub> mixtures. The same method can also be used for studying the enhanced recovery of methane by injection of CO<sub>2</sub> in shale formations.

**Supporting Information Available:** Isotherm of pure ethane in 2nm-wide pores, isotherms of surface adsorbed pure methane and pure ethane in 4nm-wide pores, isotherms of the surface adsorbed methane and ethane in 4nm-wide pores, density profiles of methane and ethane molecules inside nanopores in equilibrium with baths with different pressures, the total diffusion coefficient of methane and ethane in 2nm-wide and 4nm-wide nanopores, and the calculation of the ethane-to-methane flux ratio during gas recovery when concentration polarization is taken into account. This material is available free of charge via the Internet at <a href="http://pubs.acs.org">http://pubs.acs.org</a>.

**Acknowledgements.** We thank the ARC at Virginia Tech for generous allocations of computer time on the BlueRidge and NewRiver cluster.

## References

- 1. United States Energy Information Administration, Annual energy outlook 2013. In U.S. Department of Energy, Ed. Ishington, DC, 2013; pp 60-62.
- 2. Bulba, K. A.; Krouskop, P. E., Compositional variety complicates processing plans for US shale gas. *Oil & Gas Journal* **2009**, 107, (10), 50-55.
- 3. Javadpour, F.; Fisher, D.; Unsworth, M., Nanoscale gas flow in shale gas sediments. *Journal of Canadian Petroleum Technology* **2007**, 46, (10), 55-61.
- 4. Wang, J.; Chen, L.; Kang, Q.; Rahman, S. S., The lattice Boltzmann method for isothermal micro-gaseous flow and its application in shale gas flow: A review. *International Journal of Heat and Mass Transfer* **2016**, 95, 94-108.
- 5. Bocquet, L.; Charlaix, E., Nanofluidics, from bulk to interfaces. *Chemical Society Reviews* **2010**, 39, (3), 1073-1095.
- 6. Eijkel, J. C.; Van Den Berg, A., Nanofluidics: what is it and what can we expect from it? *Microfluidics and Nanofluidics* **2005**, 1, (3), 249-267.
- 7. Vo, T. Q.; Kim, B., Transport Phenomena of Water in Molecular Fluidic Channels. *Scientific Reports* **2016**, 6, 3 3881.
- 8. Vo, T. Q.; Barisik, M.; Kim, B., Atomic density effects on temperature characteristics and thermal transport at grain boundaries through a proper bin size selection. *The Journal of chemical physics* **2016**, 144, (19), 194707.
- 9. Vo, T. Q.; Park, B.; Park, C.; Kim, B., Nano-scale liquid film sheared between strong wetting surfaces: effects of interface region on the flow. *Journal of Mechanical Science and Technology* **2015**, 29, (4), 1681.
- 10. Bakli, C.; Chakraborty, S., Effect of presence of salt on the dynamics of water in uncharged nanochannels. *The Journal of chemical physics* **2013**, 138, (5), 054504.
- 11. Chen, L.; Zhang, L.; Kang, Q.; Viswanathan, H. S.; Yao, J.; Tao, W., Nanoscale simulation of shale transport properties using the lattice Boltzmann method: permeability and diffusivity. *Scientific Reports* **2015**, *5*, 8089
- 12. Sharma, A.; Namsani, S.; Singh, J. K., Molecular simulation of shale gas adsorption and diffusion in inorganic nanopores. *Molecular Simulation* **2015**, 41, (5-6), 414-422.
- 13. Qajar, A.; Daigle, H.; Prodanovic, M., Methane dual-site adsorption in organic-rich shale-gas and coalbed systems. *International Journal of Coal Geology* **2015**, 149, 1-8.
- 14. Li, D.; Zhang, L.; Wang, J. Y.; Lu, D., Composition-Transient Analysis in Shale-Gas Reservoirs With Consideration of Multicomponent Adsorption. *SPE Journal* **2016**, 21, (02), 648-664.

- 15. Zhang, L.; Li, D.; Li, L.; Lu, D., Development of a new compositional model with multi-component sorption isotherm and slip flow in tight gas reservoirs. *Journal of Natural Gas Science and Engineering* **2014**, 21, 1061-1072.
- 16. Fathi, E.; Akkutlu, I. Y., Multi-component gas transport and adsorption effects during CO 2 injection and enhanced shale gas recovery. *International Journal of Coal Geology* **2014**, 123, 52-61.
- 17. Chareonsuppanimit, P.; Mohammad, S. A.; Robinson, R. L.; Gasem, K. A., High-pressure adsorption of gases on shales: Measurements and modeling. *International Journal of Coal Geology* **2012**, 95, 34-46.
- 18. Weniger, P.; Kalkreuth, W.; Busch, A.; Krooss, B. M., High-pressure methane and carbon dioxide sorption on coal and shale samples from the Paraná Basin, Brazil. *International Journal of Coal Geology* **2010**, 84, (3), 190-205.
- 19. Tan, Z.; Gubbins, K. E., Selective adsorption of simple mixtures in slit pores: a model of methane-ethane mixtures in carbon. *The Journal of Physical Chemistry* **1992**, 96, (2), 845-854.
- 20. Wang, Y.; Tsotsis, T. T.; Jessen, K., Competitive Sorption of Methane/Ethane Mixtures on Shale: Measurements and Modeling. *Industrial & Engineering Chemistry Research* **2015**, 54, (48), 12187-12195.
- 21. Collell, J.; Galliero, G.; Gouth, F.; Montel, F.; Pujol, M.; Ungerer, P.; Yiannourakou, M., Molecular simulation and modelisation of methane/ethane mixtures adsorption onto a microporous molecular model of kerogen under typical reservoir conditions. *Microporous and Mesoporous Materials* **2014**, 197, 194-203.
- 22. Siperstein, F. R.; Myers, A. L., Mixed-gas adsorption. *AIChE journal* **2001**, 47, (5), 1141-1159.
- 23. Clarkson, C.; Bustin, R., Binary gas adsorption/desorption isotherms: effect of moisture and coal composition upon carbon dioxide selectivity over methane. *International Journal of Coal Geology* **2000**, 42, (4), 241-271.
- 24. Myers, A.; Prausnitz, J. M., Thermodynamics of mixed-gas adsorption. *AIChE Journal* **1965**, 11, (1), 121-127.
- 25. Wang, Z.; Guo, Y.; Wang, M., Permeability of high-Kn real gas flow in shale and production prediction by pore-scale modeling. *Journal of Natural Gas Science and Engineering* **2016**, 28, 328-337.
- 26. Lunati, I.; Lee, S., A dual-tube model for gas dynamics in fractured nanoporous shale formations. *Journal of Fluid Mechanics* **2014**, 757, 943-971.
- 27. Lee, S.; Padmanabhan, L.; Al-Sunaidi, H., Simulation of linear displacement experiments on massively parallel computers. *SPE Journal* **1996,** 1, (03), 327-340.

- 28. Chempath, S.; Krishna, R.; Snurr, R. Q., Nonequilibrium molecular dynamics simulations of diffusion of binary mixtures containing short n-alkanes in faujasite. *The Journal of Physical Chemistry B* **2004**, 108, (35), 13481-13491.
- 29. Patzek, T. W.; Male, F.; Marder, M., Gas production in the Barnett Shale obeys a simple scaling theory. *Proceedings of the National Academy of Sciences* **2013**, 110, (49), 19731-19736.
- 30. Martin, M. G.; Siepmann, J. I., Transferable potentials for phase equilibria. 1. United-atom description of n-alkanes. *The Journal of Physical Chemistry B* **1998**, 102, (14), 2569-2577.
- 31. Barisik, M.; Beskok, A., Scale effects in gas nano flows. *Physics of Fluids* **2014**, 26, (5), 052003.
- 32. Ambrose, R. J.; Hartman, R. C.; Diaz-Campos, M.; Akkutlu, I. Y.; Sondergeld, C. H., Shale gas-in-place calculations part I: new pore-scale considerations. *SPE Journal* **2012**, 17, (01), 219-229.
- 33. Plimpton, S., Fast parallel algorithms for short-range molecular dynamics. *Journal of computational physics* **1995**, 117, (1), 1-19.
- 34. Talbot, J., Analysis of adsorption selectivity in a one-dimensional model system. *AIChE journal* **1997**, 43, (10), 2471-2478.
- 35. Bakaev, V.; Steele, W., Hard rods on a line as a model for adsorption of gas mixtures on homogeneous and heterogeneous surfaces. *Langmuir* **1997**, 13, (5), 1054-1063.
- 36. Du, Z.; Manos, G.; Vlugt, T. J.; Smit, B., Molecular simulation of adsorption of short linear alkanes and their mixtures in silicalite. *AIChE journal* **1998**, 44, (8), 1756-1764.
- 37. Wu, H.; He, Y.; Qiao, R., Superdiffusive gas recovery from nanopores. *Physical Review Fluids* **2016**, 1, (7), 074101.
- 38. Skoulidas, A. I.; Sholl, D. S.; Krishna, R., Correlation effects in diffusion of CH4/CF4 mixtures in MFI zeolite. A study linking MD simulations with the Maxwell– Stefan formulation. *Langmuir* **2003**, 19, (19), 7977-7988.
- 39. Collell, J.; Galliero, G.; Vermorel, R.; Ungerer, P.; Yiannourakou, M.; Montel, F.; Pujol, M., Transport of multicomponent hydrocarbon mixtures in shale organic matter by molecular simulations. *The Journal of Physical Chemistry C* **2015**, 119, (39), 22587-22595.
- 40. Baihly, J. D.; Altman, R. M.; Malpani, R.; Luo, F. In *Shale gas production decline trend comparison over time and basins*, SPE annual technical conference and exhibition, Florence, Italy, 19-22 September, 2010; Society of Petroleum Engineers: Florence, Italy, 2010.